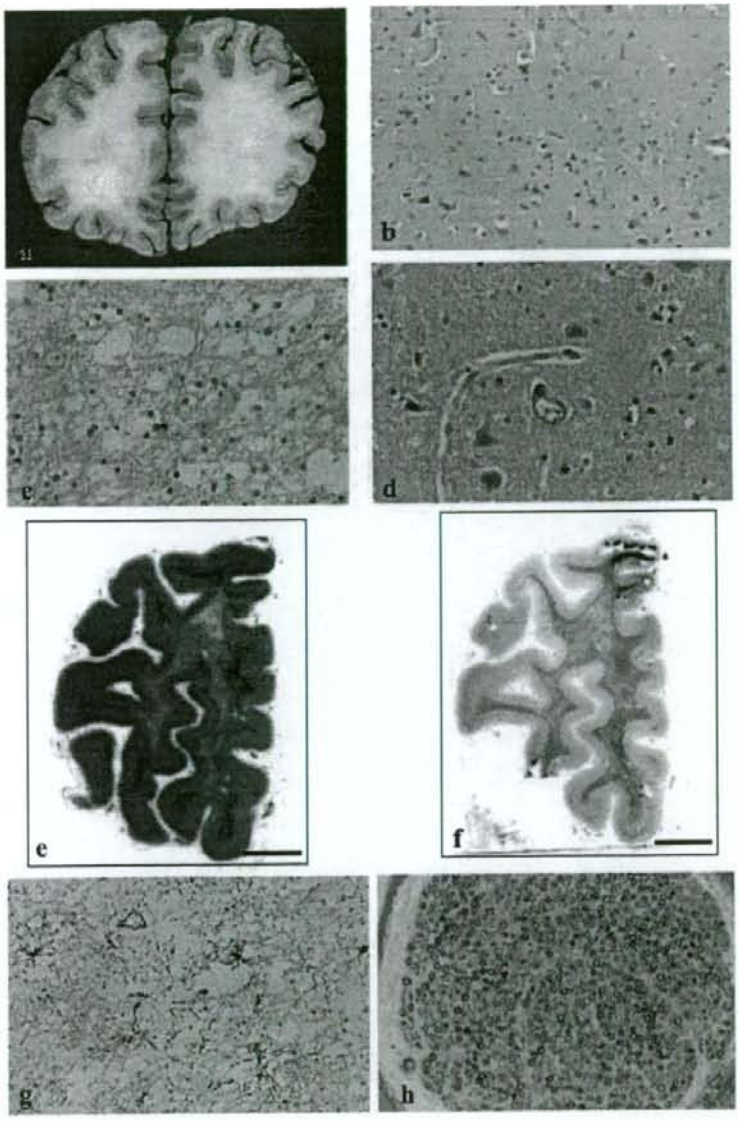

Fig. 2 (a) Multiple small lesions with greyish discoloration were scattered in the subcortical white matter. Diffuse greyish discoloration in the deep white matter. (b) Slight dilatation of perivascular and perineuronal space in the deep layer of the cerebral cortex (HE ×50). (c) Severe tissue rarefaction in white matter (HE ×100). (d) Alzheimer type II astrocytes in the cerebral cortex. (HE ×200). (e) Severe tissue rarefaction with loss of myelin in the frontal lobe (KB, scale bars 1 cm). (f) Severe tissue rarefaction with loss of axons in the frontal lobe (modified Bielschowsky, scale bars 1 cm). (g) Slight proliferation of reactive astrocytes (immunostain for GFAP ×100). (h) Biopsy specimens from sural nerve showing the loss of large myelinated fibers. (Toluidine blue, ×50).

DISCUSSION

The clinical picture in the present case was characterized by recurrent episodes of confusion, flapping tremor, cognitive impairment and polyneuropathy. Laboratory data showed slight hyperammonaemia and MRI demonstrated diffuse white matter lesions. A lysosomal enzyme, amino acid and long-chain fatty acid analysis excluded the known leukodystrophies and inherent metabolic disorders. Although conventional arterial portography identified left gastro-renal shunt, the patient showed no sign of portal hypertension or liver cirrhosis. Venous shunt was thought to be congenital, because of the lack of any prior history of abdominal disease, trauma or operation until admission. To conclude that the gastro-renal shunt contributed to neurological symptoms is difficult, because of the slight increase in serum ammonia level and small shunt vessels. The shunt vessels were large enough to develop the encephalopathy

and serum ammonia levels were high in previous reports of PSE.[9-12]

However, pathological findings were consistent with PSE, with the exception of severe tissue rarefaction due to severe loss of myelin and axons in the cerebral deep white matter. Thus PSE was diagnosed on the basis of neurological symptoms and pathological findings. Patients with PSE without portal hypertension or liver cirrhosis are often misdiagnosed with dementia or other psychoneurological diseases and occasionally hospitalized in psychiatric departments.[6] This report suggests that a slight increase in serum ammonia and very small shunt vessels might be sufficient to cause development of PSE.

Peripheral demyelinating neuropathy was one of the clinical features in our patient. Nerve conduction studies for patients with liver disease have shown that both demyelination and axonal degeneration could develop.[13] Two factors postulated for hepatic neuropathy are portal-systemic shunt and hepatocellular damage,[14] so portal-systemic shunt appears to have been involved as a cause of peripheral neuropathy in the present case.

Neuropathological findings in PSE commonly include pseudolaminar spongiform change associated with numerous Alzheimer type II astrocytes in the deep layers of cerebral cortices and loss of myelin and axons in the subcortical white matter. Alzheimer type II astrocytes are distributed to the cerebral cortex, basal ganglia and cerebellum.[15] In the present case, neuropathological evaluation also demonstrated slight dilatation of perivascular and perineuronal spaces in the cerebral cortex with some Alzheimer type II astrocytes, which displayed a limited distribution to the cerebral cortex and basal ganglia. These findings may be attributed to a slight increase in serum ammonia levels due to small shunt vessels. In addition, degeneration of deep white matter with diffuse tissue rarefaction was a unique pathological finding, corresponding to hyperintensity on T2-weighted MRI. We suggest that the portal-systemic shunt participated in the development of cerebral white matter lesions, which expanded with disease progression. Although we were not able to find a similar case in the literature, some MRI studies reported on the cerebral deep white matter lesions in hepatic encephalopathy.[16-18] They suggested that cerebral white matter lesions might be due to mild brain edema by the impairment of the blood–brain barrier. Several experimental studies have suggested that swelling of cerebral cortical astrocytes is observed following ammonia infusion in primates or exposure of primary astrocyte cultures to ammonia.[19,20] We speculate that tissue rarefaction in the white matter may have been caused by chronic brain edema due to dysfunction of astrocytes in the present case. Further studies are needed to clarify correlations between brain edema and astrocyte dysfunction in PSE.

REFERENCES

1. Hazell AS, Butterworth RF. Hepatic encephalopathy: an update of pathophysiologic mechanisms. *Proc Soc Exp Biol Med* 1999; **222**: 99–112.
2. Sherlock S, Summerskill WH, White LP, Phear EA. Portal-systemic encephalopathy; neurological complications of liver disease. *Lancet* 1954; **267**: 454–457.
3. White LP, Phear EA, Summerskill WH, Sherlock S. Ammonium tolerance in liver disease: observations based on catheterization of the hepatic veins. *J Clin Invest* 1955; **34**: 158–168.
4. Inose T. Hepatocerebral degeneration, a special type. *J Neuropathol Exp Neurol* 1952; **11**: 401–408.
5. Watanabe A. Portal-systemic encephalopathy in non-cirrhotic patients: classification of clinical types, diagnosis and treatment. *J Gastroenterol Hepatol* 2000; **15**: 969–979.
6. Yokota T, Tsuchiya K, Umetani K, Furukawa T, Tsukagoshi H. Choreoathetoid movements associated with a spleno-renal shunt. *J Neurol* 1988; **235**: 487–488.
7. Inoue E, Hori S, Narumi Y *et al.* Portal-systemic encephalopathy: presence of basal ganglia lesions with high signal intensity on MR images. *Radiology* 1991; **179**: 551–555.
8. Victor M, Adams RD, Cole M. The acquired (non-Wilsonian) type of chronic hepatocerebral degeneration. *Medicine* 1965; **44**: 345–396.
9. Konno K, Ishida H, Uno A, Ohnami Y, Masamune O. Large extrahepatic portosystemic shunt without portal hypertension. *Abdom Imaging* 1997; **22**: 79–81.
10. KCS, Matsutani S, Maruyama H *et al.* Portal-systemic encephalopathy in two patients without liver cirrhosis and portal hypertension. *Hepatol Res* 2002; **23**: 122–129.
11. Nishimoto Y, Hoshino H, Sato S *et al.* Extrahepatic portosystemic venous shunt without portal hypertension. *Intern Med* 1997; **36**: 886–889.
12. Watanabe M, Fukusato T. Extrahepatic portal-systemic encephalopathy without portal hypertension. *Intern Med* 1998; **37**: 716–717.
13. Kharbanda PS, Prabhakar S, Chawla YK, Das CP, Syal P. Peripheral neuropathy in liver cirrhosis. *J Gastroenterol Hepatol* 2003; **18**: 922–926.
14. Chopra JS, Samanta AK, Murthy JM, Sawhney BB, Datta DV. Role of porta systemic shunt and hepatocellular damage in the genesis of hepatic neuropathy. *Clin Neurol Neurosurg* 1980; **82**: 37–44.
15. Butterworth RF, Giguère JF, Michaud J, Lavoie J, Layrargues GP. Ammonia: key factor in the pathogenesis of hepatic encephalopathy. *Neurochem Pathol* 1987; **6**: 1–12.

16. Matsusue E, Kinoshita T, Ohama E, Ogawa T. Cerebral cortical and white matter lesions in chronic hepatic encephalopathy: MR-pathologic correlations. *AJNR* 2005; **26**: 347–351.
17. Yuki N, Yoshioka A, Yamaya Y, Saiki M, Hirose G. A case of portal-systemic shunt encephalopathy due to congenital portal vein hypoplasia presenting with abnormal cerebral white matter lesions on the MRI. *Rinsho Shinkeigaku* 2002; **42**: 544–547.
18. Minguez B, Rovira A, Alonso J, Cordoba J. Decrease in the Volume of white matter lesions with improvement of hepatic encephalopathy. *AJNR* 2007; **28**: 1499–1500.
19. Pilbeam CM, Anderson RM, Bhathal PS. The brain in experimental portal-systemic encephalopathy. I. Morphological changes in three animal models. *J Pathol* 1983; **140**: 331–345.
20. Norenberg MD, Lapham LW, Nichols FA, May AG. An experimental model for the study of hepatic encephalopathy. *Arch Neurol* 1974; **31**: 106–109.

ROLE OF UBIQUITIN-PROTEASOME PROTEOLYSIS IN MUSCLE FIBER DESTRUCTION IN EXPERIMENTAL CHLOROQUINE-INDUCED MYOPATHY

NORIYUKI KIMURA, MD; TOSHIHIDE KUMAMOTO, MD; TAKAHIRO ONIKI, MD; MIWA NOMURA, MD; KENICHIRO NAKAMURA, MD; YOSHITAKE ABE, MD ; YUSUKE HAZAMA, MD; and HIDETSUGU UEYAMA, MD

From the Department of Neurology and Neuromuscular Disorders, Faculty of Medicine, Oita University, Idaigaoka 1-1, Hasama, Yufu, Oita 879-5593, Japan

Acknowledgments: We are grateful to Ms. Y. Umeki, Ms. K. Sato, Ms. M. Ono, and Ms. K. Hirano for technical assistance.

Address reprint requests and correspondence to: Dr. Toshihide Kumamoto
Department of Neurology and Neuromuscular Disorders
Faculty of Medicine, Oita University
Idaigaoka 1-1, Hasama, Yufu, Oita 879-5593, Japan
Phone: +81 + 97 - 586 - 5814
Fax: +81 + 97 - 586 - 6502
E-mail: kumagoro@med.oita-u.ac.jp

Running head: Chloroquine-induced myopathy

ABSTRACT

Previous studies have documented the presence of rimmed vacuoles, atrophic fibers, and increased lysosomal cathepsins activity in skeletal muscle from animal models of chloroquine-induced myopathy, suggesting that muscle fibers in this myopathy may be degraded via the lysosomal proteolysis pathway. Given recent evidence of abnormal ubiquitin accumulation in rimmed vacuoles, the present study examined the significance of the ubiquitin-proteasome proteolytic system in the process of muscle fiber destruction in experimental chloroquine myopathy. Expression of ubiquitin, 26S proteasome proteins, and ubiquitin ligases, such as muscle-specific RING finger 1 (MuRF-1) and atrogin-1/muscle atrophy F-box protein (MAFbx), was analyzed in innervated and denervated rat soleus muscles after treatment with either saline or chloroquine. Abnormal accumulation of rimmed vacuoles was observed only in chloroquine-treated denervated muscles. Ubiquitin and proteasome immunostaining, and ubiquitin, MuRF-1 and atrogin-1/MAFbx mRNAs were significantly increased in denervated soleus muscles from saline- and chloroquine-treated rats when compared with contralateral, innervated muscles. Further, ubiquitin and ubiquitin ligase mRNA levels were higher in denervated muscles from chloroquine-treated rats when compared with saline-treated rats. These data demonstrate increased proteasomes and ubiquitin in denervated muscles from chloroquine-treated rats and suggest that the ubiquitin-proteasome proteolysis pathway as well as the lysosomal proteolytic pathway mediate muscle fiber destruction in experimental chloroquine myopathy.

Key words: chloroquine, ubiquitin, denervation, rimmed vacuoles, MuRF-1, atrogin-1/MAFbx

INTRODUCTION

The autophagic-lysosome system plays an important role in the degradation and turnover of intracellular proteins and organelles in skeletal muscles.[5] Chloroquine, a lysosomotropic agent, mediates autophagic protein degradation in this autophagic-lysosome system and promotes accumulation of sequestered materials in the autophagosome by terminating protein degradation in the lysosome system. Indeed, chloroquine-treated muscle display rimmed vacuoles of dense granular bodies and vacuoles, which include variably sized and shaped autophagosomes.[11,20]

The rimmed vacuole is the pathological hallmark in chloroquine myopathy in human and animals. Given the frequency of rimmed vacuoles in various myopathies such as distal myopathy with rimmed vacuoles (DMRV) and inclusion body myopathy (IBM), it is important to gain an understanding of mechanism and regulation involved in their formation. We previously demonstrated that denervation induces the marked accumulation of rimmed vacuoles in experimental chloroquine-induce myopathy, although in human chloroquine myopathy there may be not such a condition except for incidental denervation as with compression radiculopathy due to spongilosis. Namly, we observed an increased number of rimmed vacuoles and severe atrophic fibers in denervated chloroquine-treated rat muscles as well as the absence of these findings in contralateral, innervated chloroquine-treated muscle and in the innervated muscles of saline-treated rats.[13] Further, immunostaining for cathepsins B and L (lysosomal protease) was increased in denervated muscle from chloroquine-treated rats, suggesting that degenerative process in this myopathy progress is mediated by the lysosomal autophagic process.[13] Since both an autophagic-lysosome process and a nonlysosomal process (i.e., calpain and ubiquitin-proteasome proteolytic pathways)[15,22] mediate degradation of muscle fibers in denervated muscles,[12] chloroquine-induced dysfunction of the autophagic-lysosome process could represent an excellent mechanistic explanation for vacuole formation.[13]

In DMRV-and IBM, rimmed vacuoles and some vacuole-free fibers contain abnormally high amounts of ubiquitin,[1,12] which modifies cellular proteins and targets abnormal or normal proteins for highly selective breakdown by an ATP-dependent pathway.[10,16] Recent evidence has indicated that the nonlysosomal ATP-ubiquitin-dependent proteolytic protease, as a multicatalytic protease complex (proteasome), can meditate muscle wasting in the context of various catabolic states.[10,16,23] Degradation of a protein via this pathway involves two distinct steps: signaling by the covalent attachment of multiple ubiquitin molecules, followed by degradation of the targeted protein by an ATP-dependent protease, the 26S (1,500 kDa) proteasome,[23] with the subsequent release of free, reutilizable ubiquitin. The proteasome is found in both the cytoplasm and the nucleus of muscle cells and may be responsible for muscle fiber degradation.[2,9,10,15] Further, ATP-ubiquitin-dependent proteolytic pathway is responsible for the bulk of muscle protein breakdown, including that of myofibrillar proteins (e.g., myosin and actin) during various physiological and pathological conditions (e.g., starvation, denervation, metabolic acidosis, and sepsis).[2,9,10,15]

Proteins degraded by the ubiquitin-proteasome proteolytic pathway are first conjugated to multiple molecules of ubiquitin.[6,9,10,17] This reaction requires the activation of ubiquitin by the ubiquitin activating enzyme (E1), transfer to an ubiquitin conjugating enzyme (E2), and subsequent linkage to the lysine residue in proteins destined for degradation. The latter reaction is catalyzed by the ubiquitin ligases (E3).[6,9,10,17] This series of reactions is repeated until the target protein is labeled with a polyubiquitin chain. The polyubiquitin-conjugated proteins are recognized by the 19S subunit of the proteasome and subsequently degraded into peptides in the 20S proteasome core. Among these enzymes, different members of the E2 and ubiquitin ligase families work in concert and account for substrate and tissue specificity [9, 13].[9,10] Recent studies suggest that in addition to E3α, other ubiquitin ligases, including muscle specific RING finger 1 (MuRF-1) and atrogin-1/muscle atrophy F-box protein (MAFbx), may regulate muscle protein breakdown in various catabolic conditions and may actually be more important

than E3α for the development of muscle wasting.[3,14,17,25] In fact, these ubiquitin ligases are increased in skeletal muscle atrophy induced by nutrient deprivation, unloading, diabetes, uremia, and cancer.[3,14,17] Bodine et al. reported that the gene expression of the ubiquitin ligases MuRF-1 and MAFbx was substantially upregulated in rat skeletal muscle after institution of conditions that are all associated with a significant loss of muscle mass,[25] including immobilization, denervation, hind limb suspension, or treatment with interleukin-1 or dexamethasone.[3]

Although the influence of certain catabolic condition on the expression of MuRF-1 and atrogin-1/ MAFbx in skeletal muscles has previously been reported [15, 18], the expression of these genes in skeletal muscles from chloroquine-induced myopathy is not known. Thus the goal of this study was to characterize the significance of the ubiquitin-protease-dependent proteolytic pathway in muscle fiber destruction by conducting immunohistochemical and real-time reverse transcriptase-polymerase chain reaction (RT-PCR) studies on the innervated and denervated skeletal muscles from saline- and chloroquine-treated rats.

MATERIALS AND METHODS

Animals. The left hind-legs of 40 adult male Wistar rats (200-250 g) were denervated by ligation of the sciatic nerve, as previously described.[13] Chloroquine chloride (50 mg/kg body weight) was injected intraperitoneally into 20 rats twice daily, beginning on the day after denervation. The remaining 20 rats received injection of saline. The soleus muscles from the right (innervated) and left (denervated) legs were obtained from the chloroquine- and saline-treated rats on days 4, 8 and 16 after the initial injection. The muscles were then rapidly frozen in isopentane cooled in liquid nitrogen.

Histologic and immunohistochemical studies. Routine histologic analysis was performed using cryostat sections (10-μm thick), as described previously.[12,13] Hematoxylin-eosin preparations of each specimen were analyzed with a Nikon Cosmozon ISA image analyzer (Nikon, Tokyo, Japan) attached to a Macintosh computer (Apple Computer, Cupertino, Calif., USA). The number of fibers with dense granular bodies or vacuoles at the light microscopic level was determined in 400 muscle fibers per muscle.

For immunofluorescence analysis, frozen tissue section were fixed in 4% paraformaldehyde for 20 min. For antigen retrieval, sections were immersed in 10 mM sodium citrate buffer, pH 6.0 (Iatron, Tokyo, Japan), autoclaved at 120°C for 10 min and cooled to room temperature. Unstained sections were incubated overnight at 4°C with a monoclonal antibody for the 20S proteasomes (diluted 1:50; Santa Cruz Biotechnology, Santa Cruz, Calif., USA) or for ubiquitin (diluted 1:200; Chemicon International, Temecula, Calif., USA). After washing, Alexa Fluor 488-labeled goat anti-mouse immunoglobulin G (IgG; H + L)(diluted 1:250; Molecular Probes, Eugene, Oreg., USA) was added respectively for 1 h. Specimens were mounted on slides for visualization by fluorescence microscopy. Images were captured using a Carl Zeiss LSM5 Pasal-V3.2 confocal laser scanning microscope (Carl Zeiss, Oberkochen, Germany).

Immunostaining was specific because there was no staining when sections were allowed to react without the first-layer antibodies or when normal goat serum was substituted for the antibody.

Real-time RT-PCR. Innervated and denervated soleus muscles from saline- and chloroquine-treated rats were excised and frozen rapidly in liquid nitrogen, and stored at -80°C until use. Total RNA was isolated from specimens using acid guanidinium thiocyanate buffer (Nippon Gene, Tokyo, Japan), according to the manufacturer's instructions. The purity of the RNA was checked by the ratio of absorbance at 260 and 280 nm. Complementary DNA (cDNA) was synthesized from 1 μg of total RNA using 200 units of Moloney murine leukemia virus reverse transcriptase (Gibco BRL, Rockville,

Md., USA) and 1 μg of oligo- (dT) 12-18 primer (Invitrogen, Tokyo, Japan). Gene-specific primers for real-time PCR were purchased from Takara Bio Inc, (Otsu, Shiga, Japan). The nucleotide sequences of the primers used in this study were as follows: the rat MuRF-1 mRNA (Accession No. NM 080903; sense, 5'-GGG AAC GAC CGA G TT CAG ACT ATC-3'; antisense, 5'-GGC GTC AAA CTT GTG GCT CA-3'), the rat atrogin-1/MAFbx 32 mRNA (Accession No. NM 133521; sense, 5'-AGT GAA G AC CGG CTA CTG TGG AA-3'; antisense, 5'-TTG CAA AGC TGC AGG GTG AC-3'), the rat ubiquitin-C mRNA (Accession No. NM 017314; sense, 5'-GGG CAT GCA GAT CTT TGT GAA-3'; antisense, 5'-ACC TCC AGG GTG ATG GTC TTG-3'), and the rat glycerol aldehyde 3-phosphate dehydrogenase (GAPDH) mRNA (Accession No. NM 017008; sense, 5'-GAC AAC TTT GGC ATC GTG GA-3'; antisense, 5'-ATG CAG GGA TGA TGT TCT GG-3'). Quantitative real-time RT-PCR was performed using a LightCycler 2.0 instrument (Roche Diagnostics, Mannheim, Germany) and software version 4.0, respectively. The reaction mixture consisted of 1:25 diluted cDNA (5 μl), 0.2 μM of each primer, 2 μl of LightCycler FastStart DNA Master SYBR Green I mix (Roche Diagnostics) and 4 mM of $MgCl_2$ in a total volume of 20μl. The PCR conditions consisted of one denaturing cycle at 95°C for 10 min, followed by 45 cycles consisting of denaturing at 95°C for 10 s, annealing at 55°C for 10 s, and extension at 72°C for 10 s. Formation of expected PCR product was confirmed by agarose gel electrophoresis (2%) and melting curve analysis. The relative amount of mRNA expression was calculated by measuring the threshold cycle of each PCR product, compared with the GAPDH mRNA as an internal control. All PCR runs were performed in triplicate.

Statistical analysis. Differences between control specimens and disease specimens were evaluated with the unpaired *t*-test. A p-value of < 0.05 was considered statistically significant.

RESULTS

Histologic and immunohistochemical studies. Histologic findings for the innervated and denervated soleus muscles from saline- and chloroquine-treated rats on each test day were consistent with those from previous reports (Fig. 1).[13] Briefly, on days 4, 8, and 16 after the initial injection, the majority of the right innervated soleus muscles of the saline and chloroquine-treated rats appeared normal. By contrast, the left, denervated muscles of both groups showed marked neurogenic changes with varying degrees of severity, as has been described elsewhere.[13] These muscles showed moderate or severe muscle fiber atrophy. Marked accumulations of dense granular bodies or vacuoles were observed in the denervated chloroquine-treated muscles, particularly on days 8 and 16, whereas they were very rare in the denervated saline-treated muscles.

Quantitative analysis showed that the mean diameters of the fibers in the denervated muscles of the saline- and chloroquine-treated rats on day 16 (32.2 ± 7.4 μm; $21.9 \pm 6,4$ μm, respectively) were significantly smaller than those in the innervated muscles (49.7 ± 11.2 μm; 49.5 ± 10.0 μm, respectively; $P < 0.01$). Furthermore, the mean diameter of the muscle fibers in the denervated muscles of the chloroquine-treated rats was significantly smaller than that of the saline-treated rats ($P < 0.001$). By contrast, the diameters did not significantly differ when comparing the innervated muscles of the experimental animal groups.

Immunostaining for 20S proteasomes and ubiquitin was minimal in innervated muscles from saline- and chloroquine-treated rats at all time points, whereas denervated muscles from both groups showed progressively stronger staining for these proteins with increasing time (Fig. 2). Strong positive reaction for proteasomes and ubiquitin was often observed cytoplasm, primarily in small atrophic fibers and within vacuoles in the denervated muscles of chloroquine-treated rats. The qualitative immunohistochemical analysis showed that the denervated muscles of chloroquine-treated rats showed strong positive reactions when compared with the saline-treated rats. Increased ubiquitin

positive granules were observed in the sarcoplasm, especially in muscle fibers containing vacuoles and occasionally in the vacuoles themselves.

Ubiquitin and ubiquitin ligase mRNA levels. Ubiquitin, MuRF-1 and atrogin-1/MAFbx mRNA levels were measured in the innervated and denervated soleus muscles of saline- and chloroquine-treated rats at various time points (Figs. 3-5). Ubiquitin mRNA levels were unchanged in all experimental muscles on day 4 when compared with innervated muscles from saline treated rats on day 4 after initial injection. Elevation in ubiquitin mRNA levels occurred on days 8 and 16 in denervated muscles from chloroquine-treated rats (7.3 and 4.5-fold increased relative to innervated muscle from saline-treated rats on days 8 and 16, respectively; on day 8, $P < 0.05$; on day 16, $P < 0.02$). Ubiquity mRNA levels in enervated muscles from saline-treated rats were 2.6 (on day 8, $P < 0.02$) and 1.3 (on day 16, P = NS)-fold those of innervated muscles from saline-treated raps on days 8 and 16, respectively. Ubiquitin mRNA levels in the denervated muscles of chloroquine-treated rats tended to be higher than in saline-treated rats on days and 16 (on day 8, P = NS; on day 16, $P < 0.05$). Innervated muscle from chloroquine-treated rats were essentially similar when comparing innervated muscles from saline-treated rats on each test day (Fig. 3).

MuRF-1 mRNA levels in denervated muscle of saline-treated rats subsequently increased from day 4, peaked on day 8, and then decreased to the control levels at day 16. The mRNA levels in these muscles were 2.3 (on day 4, $P < 0.05$), 3.3- (on day 8, $P < 0.01$), and 1.2-fold (on day 16, P = N.S.) those of innervated muscles from saline-treated rats on days 4, 8 and 16, respectively (Fig. 4). MuRF-1 mRNA levels were increased in the denervated muscles from chloroquine-treated rats on all test days, with the respective levels on days 4, 8 and 16 being 2.9, 2.1 and 2.4-fold those of innervated muscles from saline-treated rats, respectively (on day 4, $P < 0.02$; on day 8, $P < 0.05$; on day 16, P = N.S.).

In the denervated muscles from saline-treated rats, atrogin-1/MAFbx mRNA levels abruptly increased to 7.1-fold ($P < 0.01$) those of innervated muscles from saline-treated rats on day 8 and then returned to the control muscle value on day 16. Atrogin-1/MAFbx mRNA levels in denervated muscles from chloroquine-treated rats subsequently increased from 4 day and peaked on day 16. Atrogin-1/MAFbx mRNA levels in these muscles were 2.8, 3.7 and 5.6-fold those of involved muscles from saline-treated rats on days 4, 8 and 16, respectively (on day 4, $P < 0.01$; on day 8, $P < 0.01$; on day 16, $P < 0.05$) (Fig. 5). MuRF-1 and atrogin-1/MAFbx mRNA levels in denervated muscles from chloroquine-treated rats were lower and higher than in saline-treated animals on days 8 and 16 respectively, but the difference was not statistically significant.

DISCUSSION

The present study demonstrated an increase in the dense granular bodies and vacuoles (primarily autophagosome and, a lesser extent, autolysosomes) in the denervated soleus muscles from chloroquine-treated rats, which is consistent with previous reports.[13] An increase in vacuolar formation was observed as early as day 2, with progressive increases thereafter. In particular, chloroquine-treated denervated muscle showed severe fiber atrophy and some necrosis as well as dense granular bodies and vacuoles. Our previous electron microscopy study revealed streaming of the Z-disk, loss of normal myofilament and disruption of the normal banding patterns, in denervated muscles from chloroquine-treated rats, representing muscle fiber destruction.[13]

Like other tissues, muscle has at least three different pathways for protein breakdown: proteolytic by lysosomal proteases (e.g., cathepsins), proteolysis by nonlysosomal, intracellular Ca^{2+}-dependent proteases (e.g., calpain), and proteolysis by nonlysosomal, ATP-ubiquitin-dependent proteolytic proteases, which function as multicatalytic protease complexes (proteasomes).[7,16,23] Proteolysis by lysosomal

cathepsins and by the calpain pathway is thought to cause muscle fiber destruction in the innervated and denervated muscles from saline- and chloroquine-treated rats. However, their intracellular distribution and role have not been studied in diseased muscles, including muscle affected by denervation and chloroquine treatment. In the present study, immunohistochemical study revealed that proteasomes are present in the cytoplasm of innervated muscle from saline- and chloroquine-treated rats, although the staining intensity was very weak. By contrast, in denervated muscles specimens from chloroquine-treated rats, proteasomes were moderately to strongly expressed in atrophic and necrotic fibers, and staining activity increased during subsequent experimental days. Moreover, denervated muscles from saline-treated rats showed mild positive immunostaining for proteasomes. On qualitative immunohistochemical analysis, this staining activity tended to be stronger in denervated muscles from chloroquine-treated rats than in saline-treated rats. Immunoreactivity for ubiquitin was occasionally positive in the cytoplasm of these atrophic fibers. Therefore, the increased staining for proteasome in atrophic fibers may be the result of up-regulation of proteasome expression, which suggests that the ubiquitin-proteasome proteolytic pathway may be responsible for muscle fiber destruction of denervated muscles, especially in those of chloroquine-treated rats.

The MuRF-1 and atrogin-1/MAFbx-expressing genes are only present in muscle tissues, indicative that these ubiquitin ligases are muscle specific. MuRF-1 is probably bound to the Z-disk by heterodimerization with MuRF-3.[19] Williams et al.[24] proposed recently, i.e., an early and perhaps rate-limiting disruption of the Z-disk and the anchorage of actin and myosin to the Z-disk with release of the myofilaments from the sarcomere making them substrates for the N- and rule pathway. MuRF-1 is speculated to play a role in the ubiquitination and degradation of titin and perhaps other proteins in the Z-disk, resulting in disruption of the Z-disk and release of actin and myosin.[25] Atrogin-1/MAFbx specifically regulates protein breakdown in skeletal muscles under the catabolic condition of denervation, immobilization, treatment with interleukin-1 or dexamethasone, sepsis, fasting, and renal failure.[3,7,25] In the present study, we found that gene expression of

newly described ubiquitin ligases the MuRF-1 and atrogin-1/MAFbx is significantly increased in the denervated soleus muscles of saline- and chloroquine-treated rats, when compared with that of the innervated muscles from both groups. This result speculates the expression of ubiquitin ligase proteins such as MuRF-1 and atrogin-1/MAFbx may be increased by denervation treatment alone and has a specific role in myofibrillar proteins degradation in the denervated muscles of saline- and chloroquine-treated rats.

The present study demonstrated that the mRNA levels of MuRF-1 and atrogin-1/MAFbx were significantly increased on day 8 in the denervated muscles of saline- and chloroquine-treated rats relative to those in the innervated muscles from saline-treated rats. They tended to be higher in denervated saline-treated rats than in denervated chloroquine-treated animals, although the difference was no statistically significant. This result speculates that the abrupt elevation of ubiquitine ligase mRNA levels might be slightly decreased in the earlier stage of muscle fiber degradation by denervation when compare with denervation alone treated rats, because of slow degradation rat or turnover of intracellular proteins, lipids, glycogen and organelles via autophagic-lysosomal system by chloroquine treatment. However, on day 16, mRNA levels in the denervated muscles from saline-treated rats decreased to the same level as that in the innervated saline-treated muscles, whereas that in the denervated muscles from chloroquine-treated rats remained unchanged. This result suggests that over the 7 days after initial ligation of the sciatic nerve, denervation induced progressive muscle atrophy, resulting in a marked increase in mRNA levels of muscle-specific ubiquitin ligase molecules. Since axonal sprouting (*i.e.*, reinnervation) is a rapid process that is completed with 2 weeks after partial denervated of rat soleus muscle,[21] a decrease of these mRNA levels in the denervated muscles of saline-treated rats on day 16 may be due to the end of denervation-induced muscle fiber degradation.

The mRNA levels of ubiquitin, MuRF-1and atrogin-1/MAFbx were increased to a greater extent in the denervated muscles from chloroquine-treated rats when compared with those from saline-treated rats on day 16, although reinnervation occurred in

chloroquine group. The simplest interpretation of these findings is that chloroquine-muscle atrophy is still progressing even on day 16. Therefore, chloroquine treatment promotes activation of ubiquitin, MuRF-1 and atrogin-1/MAFbx and their upregulation may enhance the ubiquitin-proteasome proteolytic pathway, with subsequent induction of muscle fiber destruction in the denervated soleus muscle from chloroquine-treated rats.

The present study demonstrated the ubiquitin mRNA levels increased in denervated muscles from chloroquine-treated rats but remained the same in denervated muscles from saline-treated rats. Immunohistochemical analysis for ubiquitin confirmed this difference; staining activity was stronger in the denervated muscles from chloroquine-treated rats when compared with that from saline-treated rats. The mechanism underlying this difference in ubiquitin expression remains unclear.

In conclusion, these data suggest that skeletal muscle atrophy and muscle fiber destruction occur through increased activity of the ubiquitin-proteasome proteolytic pathways in chloroquine-treated muscle after denervation. Recent studies have demonstrated that insulin-like growth factor 1 (IGF-1) stimulates muscle protein synthesis and hypertrophy via the phosphatidylinositol 3-kinase-Akt pathway, and activation of this pathway can reduce muscle atrophy.[4,18] IGF-1 rapidly suppresses atrogin-1 and polyubiquitin expression and also suppresses MuRF-1.[4] Therefore, future study to determine whether IGF-1 can suppress muscle fiber atrophy and destruction in this myopathy would be of benefit.

REFERENCES

1. Askanas V, Engel WK, Mirabella M. Idiopathic inflammatory myopathies: inclusion-body myositis, polymyositis, and dermatomyositis. Curr Opin Neurol 1994;7:448-456.
2. Beyette JR, Mykles DL. Immunocytochemical localization of the multicatalytic proteinase (proteasome) in crustacean striated muscles. Muscle Nerve 1992;15:1023-1035.
3. Bodine SC, Latres E, Baumhueter S, Lai VK, Nunez L, Clarke BA, Poueymirou WT, Panaro FJ, Na E, Dharmarajan K, Pan ZQ, Valenzuela DM, DeChiara TM, Stitt TN, Yancopoulos GD, Glass DJ. Identification of ubiquitin ligases required for skeletal muscle atrophy. Science 2001;294:1704-1708.
4. Bodine SC, Stitt TN, Gonzalez M, Kline WO, Stover GL, Bauerlein R, Zlotchenko E, Scrimgeour A, Lawrence JC, Glass DJ, Yancopoulos GD. Akt/mTOR pathway is a crucial regulator of skeletal muscle hypertrophy and can prevent muscle atrophy in vivo. Nat Cell Biol 2001;3:1014-1019.
5. Gerard KW, Hipkiss AR, Schneider DL. Degradation of intracellular protein in muscle. Lysosomal response to modified proteins and chloroquine. J Biol Chem 1988;263:18886-18890.
6. Glickman MH, Ciechanover A. The ubiquitin-proteasome proteolytic pathway: destruction for the sake of construction. Physiol Rev 2002;82:373-428.
7. Goll DE, Kleese WC, Kumamoto T, Cong J, Szpacenko A. In search of the regulation and function of the Ca^{2+}-dependent proteinases (calpain) . In: Katunuma N, Kominami E (eds). Intracellular proteolysis, mechanism and regulation. Japanese Scientific Societies press, Tokyo, 1989, pp82-91.
8. Gomes MD, Lecker SH, Jagoe RT, Navon A, Goldberg AL. Atrogin-1, a muscle-specific F-box protein highly expressed during muscle atrophy. Proc Natl Acad Sci USA 2001;98:14440-14445.

9. Hasselgren PO, Fischer JE. The ubiquitin-proteasome pathway: review of a novel intracellular mechanism of muscle protein breakdown during sepsis and other catabolic conditions. Ann Surg 1997;225:307-316.

10. Hershko A, Ciechanover A. The ubiquitin system. Annu Rev Biochem 1998;67:425-479.

11. Kumamoto T, Araki S, Watanabe S, Ikebe N, Fukuhara N. Experimental chloroquine myopathy: morphological and biochemical studies. Eur Neurol 1989;29:202-207.

12. Kumamoto T, Fujimoto S, Nagao S, Masuda T, Sugihara R, Ueyama H, Tsuda T. Proteasomes in distal myopathy with rimmed vacuoles. Intern Med 1998;37:746-752.

13. Kumamoto T, Ueyama H, Watanabe S, Murakami T, Araki S. Effect of denervation on overdevelopment of chloroquine-induced autophagic vacuoles in skeletal muscles. Muscle Nerve 1993;16:819-826.

14. Lecker SH, Jagoe RT, Gilbert A, Gomes M, Baracos V, Bailey J, Price SR, Mitch WE, Goldberg AL. Multiple types of skeletal muscle atrophy involve a common program of changes in gene expression. FASEB J 2004;18:39-51.

15. Medina R, Wing SS, Goldberg AL. Increase in levels of polyubiquitin and proteasome mRNA in skeletal muscle during starvation and denervation atrophy. Biochem J 1995;307:631-637.

16. Mitch WE, Goldberg AL. Mechanisms of muscle wasting. The role of the ubiquitin-proteasome pathway. N Engl J Med 1996;335:1897-1905.

17. Razeghi P, Baskin KK, Sharma S, Young ME, Stepkowski S, Essop MF, Taegtmeyer H. Atrophy, hypertrophy, and hypoxemia induce transcriptional regulators of the ubiquitin proteasome system in the rat heart. Biochem Biophys Res Commun 2006;342:361-364.

18. Sacheck JM, Ohtsuka A, McLary SC, Goldberg AL. IGF-I stimulates muscle growth by suppressing protein breakdown and expression of atrophy-related ubiquitin ligases, atrogin-1 and MuRF1. Am J Physiol Endocrinol Metab 2004;287:E591-601.

19. Spencer JA, Eliazer S, Ilaria RL Jr, Richardson JA, Olson EN. Regulation of microtubule dynamics and myogenic differentiation by MURF, a striated muscle RING-finger protein. J Cell Biol 2000;150:771-784.

20. Stauber WT, Hedge AM, Trout JJ, Schottelius BA. Inhibition of lysosomal function in red and white skeletal muscles by chloroquine. Exp Neurol 1981;71:295-306.

21. Thompson W, Jansen JK. The extent of sprouting of remaining motor units in partly denervated immature and adult rat soleus muscle. Neuroscience 1977;2:523-535.

22. Ueyama H, Kumamoto T, Fujimoto S, Murakami T, Tsuda T. Expression of three calpain isoform genes in human skeletal muscles. J Neurol Sci 1998;155:163-169.

23. Voisin L, Breuille D, Combaret L, Pouyet C, Taillandier D, Aurousseau E, Obled C, Attaix D. Muscle wasting in a rat model of long-lasting sepsis results from the activation of lysosomal, Ca^{2+} -activated, and ubiquitin-proteasome proteolytic pathways. J Clin Invest 1996;97:1610-1617.

24. Williams AB, Decourten-Myers GM, Fischer JE, Luo G, Sun X, Hasselgren PO. Sepsis stimulates release of myofilaments in skeletal muscle by a calcium-dependent mechanism. FASEB J 1999;13:1435-1443.

25. Wray CJ, Mammen JM, Hershko DD, Hasselgren PO. Sepsis upregulates the gene expression of multiple ubiquitin ligases in skeletal muscle. Int J Biochem Cell Biol 2003 ;35:698-705.

Abbreviations

MuRF-1, muscle-specific RING finger 1; MAFbx, muscle atrophy F-box protein; DMRV, distal myopathy with rimmed vacuoles; RT-PCR, Semiquantitative reverse transcriptase polymerase chain reaction; IgG, immunoglobulin G; cDNA, Complementary DNA; GAPDH , glycerol aldehyde 3-phosphate dehydrogenase; IGF-1, insulin-like growth factor 1